Complete electroelastic set for the (YXt)-45 cut of a KNbO3 single crystal

R Rouffaud, P. Marchet, Anne-Christine Hladky, C. Bantignies, M. Pham-Thi, F. Levassort

JOURNAL OF APPLIED PHYSICS **116**, 194106 (2014)

Complete electroelastic set for the (YXt)-45° cut of a $KNbO_3$ single crystal

R. Rouffaud,[1,2] P. Marchet,[3] A.-C. Hladky-Hennion,[2] C. Bantignies,[4] M. Pham-Thi,[5] and F. Levassort[1,a)]

[1]*François-Rabelais University, GREMAN UMR 7347 CNRS, 37071 Tours, France*
[2]*IEMN UMR 8520 CNRS, ISEN department, 59046 Lille, France*
[3]*Limoges University, SPCTS UMR 7315 CNRS, 87068 Limoges, France*
[4]*Vermon SA, 37038 Tours, France*
[5]*Thales Research and Technology, 91767 Palaiseau, France*

(Received 21 July 2014; accepted 9 November 2014; published online 20 November 2014)

A complete and consistent set (elastic, dielectric, and piezoelectric tensors) of a commercial lead-free (YXt)-45° cut $KNbO_3$ single crystal is reported. These data were obtained using several samples and the resonance-antiresonance method. Particular attention was paid to the consistency of this delivered database. A genetic algorithm with an appropriate criterion was used. Electromechanical characterization revealed a high thickness coupling factor of approximately 60%. These properties make this single crystal a good candidate for several applications such as medical imaging. This complete set provides a basis for simulation designs of such devices integrating this piezoelectric lead-free material, especially for ultrasonic transducers. © *2014 AIP Publishing LLC*.
[http://dx.doi.org/10.1063/1.4902168]

I. INTRODUCTION

For decades, PZT ceramics[1] and its derived compositions have dominated the market due to their high piezoelectric properties and efficient production processes. PMN-PT and PZN-PT single crystals deliver even higher piezoelectric coefficients, such as d_{33}, and coupling factors such as k_{33} over 90%.[2] Currently, these materials are integrated in a wide range of devices and, in particular, in ultrasonic applications (transducers for non-destructive testing—NDT, underwater sonar systems and medical imaging). The increasing success of these materials is associated with health and environmental problems due to the presence of lead. Today, many countries and organizations worldwide are restricting or including in their legislation hazardous substances to be substituted by safer alternatives.[3] Among the most researched lead-free compositions are perovskite barium titanate, alkaline niobates, and bismuth sodium titanates.[4–6] Particular attention has been paid to $(K_{0.5}Na_{0.5})NbO_3$ (KNN) ceramics due to their high piezoelectric coefficients and high Curie temperatures. Like lead-based compositions, lead-free single crystals can also deliver very high electromechanical performances depending on the selection of the poling and crystallographic directions. Moreover, some domain-engineering methods can also be used to enhance the piezoelectric properties. Several options already exist with $KNbO_3$ or $BaTiO_3$[7] single crystals. In particular, the interest in $KNbO_3$ is not new, as the first publications date from the 1970s for optic, electro-optic, and mechanical applications.[8–11] Wiesendanger proposed the first piezoelectric characteristics of this material.[10] Then, Zgonik *et al.* completed this characterization with piezoelectric and optic measurements to provide additional properties for the same material.[12] In 2000, Nakamura and Kawamura performed a study on the orientation dependence of the piezoelectric properties of $KNbO_3$ and used different cuts to optimize specific electromechanical coupling factors.[13] For medical imaging applications, length-extensional (k_{33}) and thickness-extensional (k_t) modes are commonly used. Values of 83% and 69%, for k_{33} and k_t, respectively, have been theoretically obtained. Finally, several experimental cuts from Nakamura's work were used to verify selected coupling coefficient values.[14,15] Davis *et al.* characterized monodomain and polydomain single crystals only in thickness mode. These authors also performed a frequential study that confirmed that this material is suitable for high-frequency applications.

In this paper, we focus on the (YXt)–45° cut, using IEEE standard notation,[16] in the orthorhombic frame, which allows us to favor both coupling factors k_{33} and k_t simultaneously. This cut is identical to the cut described by Davis *et al.*[15] The microstructure of a (YXt)–45° cut $KNbO_3$ crystal from FEE GmbH (Ref. 17) is first studied. Then, material characterization is performed using the resonance-antiresonance method[16] to obtain a complete set of elastic, dielectric, and piezoelectric constants. The method proposed is the same approach as those already used for several single crystal characterizations.[18] As it is often the case for the establishment of a complete set of material constants, the authors mix measured and calculated values. This can lead to violations in the interrelations between particular groups of electromechanical constants.[19] Then, a non-consistent database is provided, which may have significant consequences on the accuracy of the simulations performed for the design of new devices integrating these piezoelectric materials. In this study, a method using a genetic algorithm is proposed to optimize the consistency of a full set of material through the minimization of a defined criterion. Finally, this complete set was used to calculate the orientational dependence of the velocities and coupling factors in three different planes.

a)Electronic mail: franck.levassort@univ-tours.fr

II. MATERIALS AND METHODS

A. Crystal structure and orientation

$KNbO_3$ is orthorhombic and belongs to the mm2 point group. The corresponding space group is Bmm2 (S.G. N°38), with lattice parameters a = 5.697 Å, b = 3.971 Å, and c = 5.723 Å.[8] This structure is similar to the orthorhombic polymorph of $BaTiO_3$. The distortion is characterized by A and B cations displacements from the centers of coordination of the polyhedra, without tilting. $KNbO_3$ structure lattice parameters are related to those of the aristotype perovskite pseudo-cubic structure by the relationships $a \simeq a_p\sqrt{2}$, $b = a_p$, and $c \simeq a_p\sqrt{2}$. The reference system of this space group corresponds to the description previously used by Zgonik *et al.*[12] and by Nakamura *et al.*[14] in their study of the electromechanical properties. In this reference system, the spontaneous polarization P_s is collinear to the two-fold axis, directed along the "c" direction. The "b" lattice parameter is the shortest one, parallel to one pseudo-cubic direction, while the "a" and "c" axes form an angle of 45° with the pseudo-cubic axes (Fig. 1).

As indicated by the supplier, the crystal is oriented in such a way that the direction is perpendicular to the largest face of the crystal (thickness direction Z) lies along the bisectrix of the "a" and "c" axes, with the "b" axis lying along one edge of the crystal (Fig. 2). This orientation was verified for one of the thin electroded samples (plate shape with gold electrodes) used for electromechanical characterization using a four-circle diffractometer (Nonius Kappa CCD). The obtained lattice parameters correspond quite well to the reported values.

According to this orientation, the largest face of the sample studied corresponds to [101] planes. This sample was thus studied using conventional $\theta/2\theta$ X-ray diffraction (Bruker D8 advance, Cu Kα1, $\lambda = 0.15406$ nm) to check for a single orientation. The results are represented in log scale, in order to reveal peaks of low intensity (Fig. 3). In addition to the peaks associated to the gold electrode (stars), only four $KNbO_3$ diffraction peaks are observed: (i) two sharp (101) and (202) peaks (FWHM = 0.05°) and (ii) two broader (010) and (020) peaks of lower intensity. As a matter of comparison, the relative intensities for a randomly oriented powder (normalized to 100) are also represented in lower part of Fig. 3, together with their indexing in Bmm2 space group.

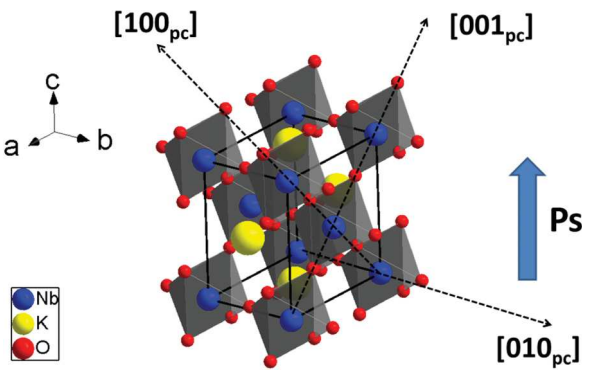

FIG. 1. Unit cell of orthorhombic $KNbO_3$ (Bmm2 space group) and correspondence of orthorhombic crystal axes with respect to the pseudo-cubic axes.

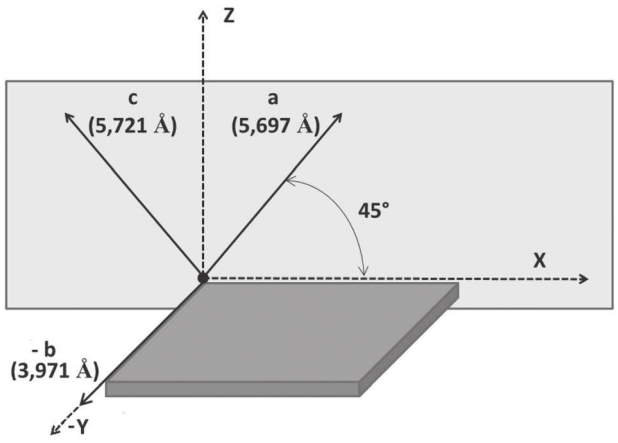

FIG. 2. Orientation frame (XYZ) of the studied crystal according to the crystallographic axes.

For powder, the most intense peak is the (111) (100%, $2\theta = 31.579°$). The (101) and (010) peaks ($2\theta = 22.001°$ and 22.370°), respectively, present relative intensities of 44.4% and 21.7%. In our case, the absence of all the diffraction peaks, except the (101), (010), (202), and (020) agrees with the study of a (almost) single crystal sample. The two sharp (101) and (202) peaks confirm that the surface studied corresponds to (101) planes, according to the crystal orientation. In addition, (010) and (020) peaks are also detected, evidencing for a (010) secondary orientation. As a consequence, we cannot consider this crystal as being totally single domain. The intensity ratio of the (101) to (010) peaks is 40.8, against 2.05 for powder. Thus, this secondary orientation represents only a small part of the crystal, indicating a minor contribution to the physical properties.

B. Electromechanical characterization

For the study of the KN single crystal, several samples needed to be cut from the sample purchased ($10 \times 10 \times 3\,mm^3$). To determine the elastic, piezoelectric, and dielectric constants from the $KNbO_3$ single crystal, the resonance-antiresonance method was used. As illustrated in Fig. 4, the original piece is used to fabricate the IEEE standard samples[16] (numbered from 1 to 5) for electromechanical characterization. The samples were cut to favor resonance modes for which the analytic electromechanical coupling factor is known. The characterized modes from these samples appear in the range from 5 MHz to 15 MHz. The experimental set-up used to measure the electrical impedance is composed of an HP4395A spectrum analyzer with its impedance test kit and specific spring clip fixture.

The components from the dielectric tensor at constant strain ϵ^S were measured from the capacitance value at twice the anti-resonance frequency with samples 1 for ϵ^S_{33} and 5 for ϵ^S_{11}. For ϵ^S_{22}, another sample is used (only for this measurement) and it is similar to number 5 but in the *Y*-direction. Components ϵ^T_{11} and ϵ^T_{33} from the dielectric tensor at constant stress were deduced thanks to k_{15} and k_t. The electromechanical

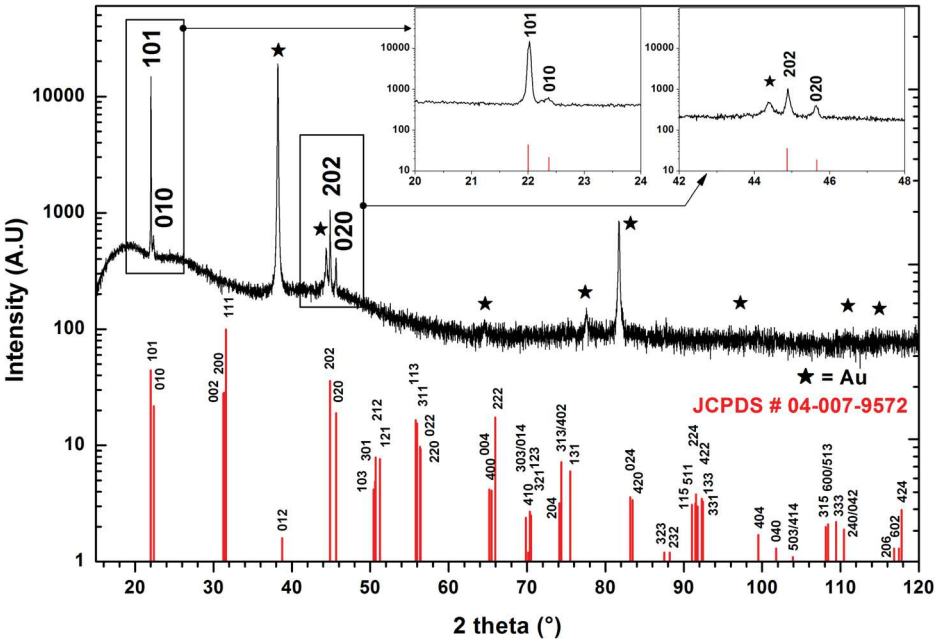

FIG. 3. X-ray diffraction pattern obtained on the surface of one platelet (log scale, $\theta/2\theta$ configuration, Cu Kα1, $\lambda = 0.15406$ nm, stars = Au gold electrodes), showing the (101) main orientation, together with (010) secondary orientation. In red, the intensities of the diffraction peaks for $KNbO_3$ powder (JCPDS card 04-007-9572).

coupling factors k_t, k_{33}, k_{15}, k_{31}, and k_{32} were measured from the resonance-antiresonance frequencies. Finally, the elastic constants s^E_{11}, s^E_{12}, s^E_{22}, s^E_{33}, s^D_{33}, c^E_{33}, c^D_{33}, c^E_{55}, and c^D_{55} and piezoelectric constants e_{33}, e_{15}, d_{31}, d_{32}, and d_{33} were deduced.[20]

C. Consistency of the complete set

1. Quantification criterion

Generally, for a complete set of materials, the values calculated are determined using some of the 16 possible intercoefficient relations summarized in Table I. For example, to determine the c^E tensor (elastic constant at constant electric field), relations (5), (7), and (14) can be used; however, practically, one is enough. If only one of these relations is selected, the corresponding parameters will be favored. To obtain a consistent set of tensors, all the intercoefficient relations must be respected considering the measured values.

Each intercoefficient relation from Table I is an equality of 2 matrices noted L, for the left member, and R, for the right member for further study. The dimensions of these matrices differ depending on the intercoefficient relation used (3×3, 3×6, or 6×6). Then, a term-by-term comparison between L and R is performed by one division to overcome problems due to the different orders of magnitude. Finally, the C-matrix, or the comparison matrix, corresponding to the intercoefficient relation k, with $k \in$,[1,16] is built to keep positive components (so two possibilities for the division) as follows:

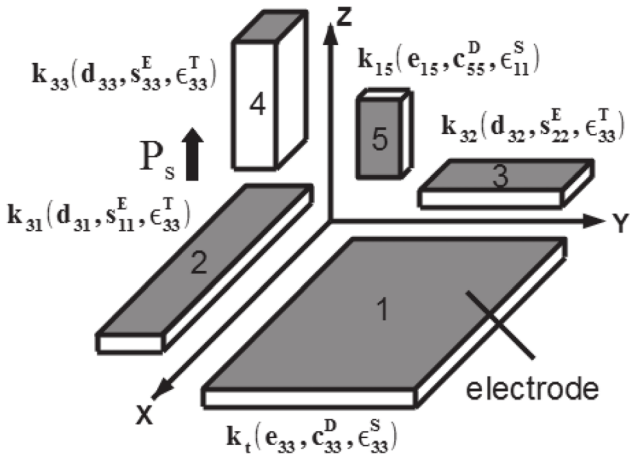

FIG. 4. Samples numbered from 1 to 5 in the frame (XYZ). The grey part corresponds to the electrodes.

TABLE I. Intercoefficient relations given in the Voigt notation.[20] Subscripts k, l, and m (respectively, n, p, and q) range from 1 to 3 (respectively, from 1 to 6).

$$\beta^S_{km}\epsilon^S_{ml} = \delta_{kl} \quad (1)$$

$$\beta^T_{km}\epsilon^T_{ml} = \delta_{kl} \quad (2)$$

$$\epsilon^T_{kl} - \epsilon^S_{kl} = d_{kn}e_{ln} \quad (3)$$

$$\beta^S_{kl} - \beta^T_{kl} = g_{kn}h_{ln} \quad (4)$$

$$c^E_{pn}s^E_{nq} = \delta_{pq} \quad (5)$$

$$c^D_{pn}s^D_{nq} = \delta_{pq} \quad (6)$$

$$c^D_{pq} - c^E_{pq} = e_{mp}h_{mq} \quad (7)$$

$$s^E_{pq} - s^D_{pq} = d_{mp}g_{mq} \quad (8)$$

$$d_{kp} = \epsilon^T_{kl}g_{lp} \quad (9)$$

$$e_{kp} = \epsilon^S_{kl}h_{lp} \quad (10)$$

$$g_{kp} = \beta^T_{kl}d_{lp} \quad (11)$$

$$h_{kp} = \beta^S_{kl}e_{lp} \quad (12)$$

$$d_{kq} = e_{kp}s^E_{pq} \quad (13)$$

$$e_{kq} = d_{kp}c^E_{pq} \quad (14)$$

$$g_{kq} = h_{kp}s^D_{pq} \quad (15)$$

$$h_{kq} = g_{kp}c^D_{pq} \quad (16)$$

$$C^k(i,j) = \begin{cases} \dfrac{L(i,j)}{R(i,j)} - 1, & \text{if } \dfrac{L(i,j)}{R(i,j)} > 1 \\ \dfrac{R(i,j)}{L(i,j)} - 1, & \end{cases} \quad (17)$$

where $i,j \in [1, N]$ and N depend on the tensor nature. For example, for the intercoefficient relations (16), the C-matrix component of the 2nd line ($i=2$) and 4th column ($j=4$) is written as follows:

$$C^{16}(2,4) = \begin{cases} h_{24}/\left(g_{24}c_{44}^D\right) - 1, & \text{if } \dfrac{h_{24}}{g_{24}c_{44}^D} > 1 \\ \left(g_{24}c_{44}^D\right)/h_{24} - 1. & \end{cases} \quad (18)$$

Each term of the C-matrix is calculated, and a zero value is considered if the term is less than 1×10^{-4} (the selected numerical accuracy). Finally, a value called p is calculated to verify the consistency. For a set of elastic, piezoelectric, and dielectric parameters, p is defined as follows:

$$p = \max_{\substack{1 \le i,j \le N \\ 1 \le k \le 16}} \{C^k(i,j)\}, \quad (19)$$

when p is 0, the set of parameters is considered as perfectly consistent (according to the chosen numerical accuracy). Consistency is important for numerical simulations such as ultrasonic device modeling using finite-element method software. Indeed, in practice, only one electro-elastic moduli (i.e., one elastic, one piezoelectric, and one dielectric tensor) is used to perform these theoretical predictions. If the full set of this material has a weak consistency (or high value of p), it means that, with a specific electro-elastic moduli (containing, for example, c^E, e, and ϵ^S), the result obtained is different from one achieved with another electro-elastic moduli (for example, s^E, d, and ϵ^T) from the same complete set. These differences introduce non-negligible errors in the theoretical results.

2. Optimization algorithm

As already mentioned, the aim of this paper is to provide a full set for the $KNbO_3$ single crystal with the best possible consistency. The values measured from part II B are fixed. Therefore, other components must be found to satisfy at best all the intercoefficient relations. This step is the optimization step. For the orthorhombic structure of the $KNbO_3$ single crystal, 68 constants from elastic, dielectric, and piezoelectric tensors must be determined. In our case, 19 measured constants are fixed in the optimization problem. Usually, to measure a maximum of constants, two methods with electromechanical and direct velocity measurements are performed jointly.[16] More especially, c_{66}^E is only determined by direct velocity measurements. However, in our case, the samples are too small to measure correct velocity values. Consequently, the c_{66}^E value is retained from the Zgonik[12] set. This value does not contribute to the calculation of p (and the consistency quantification) because it is independent of all the other constants. Finally, the 49 other missing components cannot be determined respecting at best all the intercoefficient relations. Thus, an optimization algorithm must be selected with an adequate objective function to be minimized.

Here, the genetic algorithm,[21] coded in Matlab,[22] is selected because, among the evolutionary algorithms, this algorithm is compatible with the largest number of optimization problems. Moreover, one of the main advantages of the genetic algorithm is that it is able to examine the entire search space; whereas, for a gradient flow optimization, it is possible for the process to stay in a local minimum of the objective function. Values from Zgonik *et al.*[12] were selected to restrain the search space because its $KNbO_3$ structure (monodomain) can be considered as relatively close to ours. In the optimization process, maximum variations of 200% from these values were selected. Finally, the end of the calculation is performed in accordance with a stopping criterion, which can be a defined minimum value of the objective function or the number of iterations in the optimization process. In our case, the second possibility was selected with a maximum number of 200 000 generations. This value corresponds to a good trade-off between time calculation and the delivered accuracy of the complete set.

For the objective function, it is logical to use the quantification criterion defined before and to establish the fitness value f equal to the precision p. To respect the thermodynamic stability of the orthorhombic single crystal, additional conditions established by Aleshin and Raevski[23] are also applied in the evaluation of the set of parameters.

III. RESULTS AND DISCUSSION

A. Determination of the complete set

The complete set of material parameters is given in Table II for the (XYZ) frame defined in Sec. II A. As mentioned before, 19 parameters were measured and are marked with a star. The measured electromechanical coupling coefficients k_t, k_{33}, k_{31}, k_{32}, and k_{15} are equal to 59.5%, 50.2%, 21.9%, 38.8%, and 30.3%, respectively.

The original sample, even if the sizes are relatively small, cannot be considered as a perfectly homogeneous material, which implies possible local variations of the electromechanical properties. In our case, the five samples used for the characterization most likely do not have precisely the same properties, which introduced inconsistencies in the measured data set and in the final results. Considering these inconsistencies, it is impossible to reach the perfect zero value for p. To avoid at the best the inconsistency due to the measurement on several samples, several proposed methods used only one sample with specific design for the electrodes.[24–27]

The numerical optimization described previously was executed. With the genetic algorithm, the final result does not depend on the initial database. Following the quantification criterion definition (19), the set of Table II is consistent for a precision defined by the p value 27.6×10^{-2}. This fitness value is obtained for Eq. (8) for its component $C^8(1, 1)$. The calculation of the p value can be performed with other published complete sets of piezoelectric materials with similar compositions. For comparison, the set given by Zgonik *et al.*[12] for an orthorhombic KN single crystal is consistent for a precision 263.33×10^{-2}, and Zheng *et al.*[28] reached a consistency of 8.49×10^{-2} for a tetragonal KNN-based

TABLE II. Complete set of optimized (YXt)-45° cut for $KNbO_3$ single crystal according to fundamental piezoelectric relations for various independent variable sets. Stars indicate values measured.

(S,E)-type fundamental relations: c_{ij}^E (10^9 Pa), e_{ij} (Cm^{-2}), $\epsilon_{ij}^S/\epsilon_0$								
c_{11}^E	c_{12}^E	c_{13}^E	c_{22}^E	c_{23}^E	c_{33}^E*	c_{44}^E	c_{55}^E*	c_{66}^E
212.98	36.01	67.04	105.49	47.00	191.23	74.30	123.51	95.50
e_{31}	e_{32}	e_{33}*	e_{24}	e_{15}*		ϵ_{11}^S*	ϵ_{22}^S*	ϵ_{33}^S*
3.50	−1.55	5.66	5.88	3.10		87.0	699.2	34.5
(S,D)-type fundamental relations: c_{ij}^D (10^9 Pa), h_{ij} (10^9 V m^{-1}), β_{ij}^S (10^9 mF^{-1})								
c_{11}^D	c_{12}^D	c_{13}^D	c_{22}^D	c_{23}^D	c_{33}^D*	c_{44}^D	c_{55}^D*	c_{66}^D
253.07	18.23	131.74	113.38	18.32	296.00	79.90	135.99	95.50
h_{31}	h_{32}	h_{33}	h_{24}	h_{15}		β_{11}^S	β_{22}^S	β_{33}^S
11.45	−5.07	18.47	0.95	4.02		1.30	0.16	3.25
(T,E)-type fundamental relations: s_{ij}^E (10^{-12} m^2 N^{-1}), d_{ij} (10^{-12} CN^{-1}), $\epsilon_{ij}^T/\epsilon_0$								
s_{11}^E*	s_{12}^E*	s_{13}^E	s_{22}^E*	s_{23}^E	s_{33}^E*	s_{44}^E	s_{55}^E	s_{66}^E
5.32	−1.22	−1.33	10.73	−1.88	5.25	13.46	8.10	10.47
d_{31}*	d_{32}*	d_{33}*	d_{24}	d_{15}		ϵ_{11}^T*	ϵ_{22}^T	ϵ_{33}^T*
12.73	−31.96	28.95	79.19	25.10		95.8	751.8	71.5
(T,D)-type fundamental relations: s_{ij}^D (10^{-12} m^2 N^{-1}), g_{ij} (V m N^{-1}), β_{ij}^T (10^9 mF^{-1})								
s_{11}^D	s_{12}^D	s_{13}^D	s_{22}^D	s_{23}^D	s_{33}^D*	s_{44}^D	s_{55}^D	s_{66}^D
5.00	−0.58	−1.91	9.12	−0.44	3.94	12.52	7.36	10.47
g_{31}	g_{32}	g_{33}	g_{24}	g_{15}		β_{11}^T	β_{22}^T	β_{33}^T
0.0197	−0.0504	0.0451	0.0119	0.0295		1.18	0.15	1.58
Coupling factors k (%)					Density (kg/m^3)			
k_t*	k_{33}*	k_{31}*	k_{32}*	k_{15}*	ρ*			
59.5	50.2	21.9	38.8	30.3	4575			

single crystal with less independent constants than with an orthorhombic structure.

To be more precise, $C^8(1, 1)$ corresponds to the relation (Table I)

$$s_{11}^E - s_{11}^D = d_{31}g_{31}. \tag{20}$$

If the numerical calculation is done with values from Table II, $s_{11}^E - s_{11}^D$ is 0.32 pm^2 N^{-1}, whereas $d_{31}g_{31}$ is equal to 0.25 pm^2 N^{-1}. So, the highest relative difference Δ_{max} comes from this equation with 24.25%. With Zgonik's database, Δ_{max} value is 114% and is extracted using Eq. (6) of Table I. Finally, from values of Zheng *et al.*, Δ_{max} is lower (8.2%). Among the 16 equations of Table I, the complete set of Table II agrees with 7 of them with a Δ_{max} smaller than 2%.

The measured k_{33} value (50%) is lower than that of k_t (59.5%). Generally, an inverse behavior is observed, in particular, for most lead-based single crystals such as PMN-PT or PZN-PT.[29] To confirm our results, a piezocomposite has been fabricated[30] for high frequency ultrasonic transducer applications. The measurement of k_t of this 1–3 piezocomposite before the transducer fabrication delivered a value of 47%. According to the 1–3 connectivity[31] chosen and to the single crystal volume fraction used for the composite fabrication, this value is expected to be very close to the k_{33} value of the single crystal piezoelectric phase.[32] This agrees with the observation that k_{33} is lower than k_t for our sample.

B. Functional characteristics

With the determined complete set of a $KNbO_3$ single crystal, the orientation dependence of the sound propagation velocities and electromechanical coupling coefficients based on the measured material constants given in Table II are plotted in Figs. 5 and 6. These values were calculated using the Christoffel tensor[33] and solving the corresponding eigenvalue equation for determination of the velocities.

In Fig. 5(a), which represents the velocities in the *XY*-plane, the values calculated exhibit a notable difference between the *X*-direction (6868 ms^{-1}) and the *Y*-direction (4834 ms^{-1}). In the crystal structure, a large difference between the lattice parameters "a" and "b" was measured and leads to these two values of longitudinal wave velocities. The longitudinal wave velocity in the *XZ*-plane in Fig. 5(b) confirms the small difference between the two measured lattice parameters in the *X*- and *Z*-directions. In the three planes, the shear mode velocity v_{s1} is slightly affected by the propagation direction. The longitudinal velocity reaches its maximum at 30° around the *Z*-axis in the *XZ*-plane. However, this value is very close to that on the *Z*-axis which is the propagation axis for the waves from modes generally used in the ultrasonic transduction.

The orientational dependence of the electromechanical coupling coefficients k_t, k_{33}, k_{31}, and k_{15} are represented in Fig. 6. The coupling coefficients k_{32} and k_{24} are not plotted to avoid an overload in the figure. The maxima of k_t and k_{33} are obtained along the *Z*-direction. In Fig. 6(a), the k_t and k_{33}

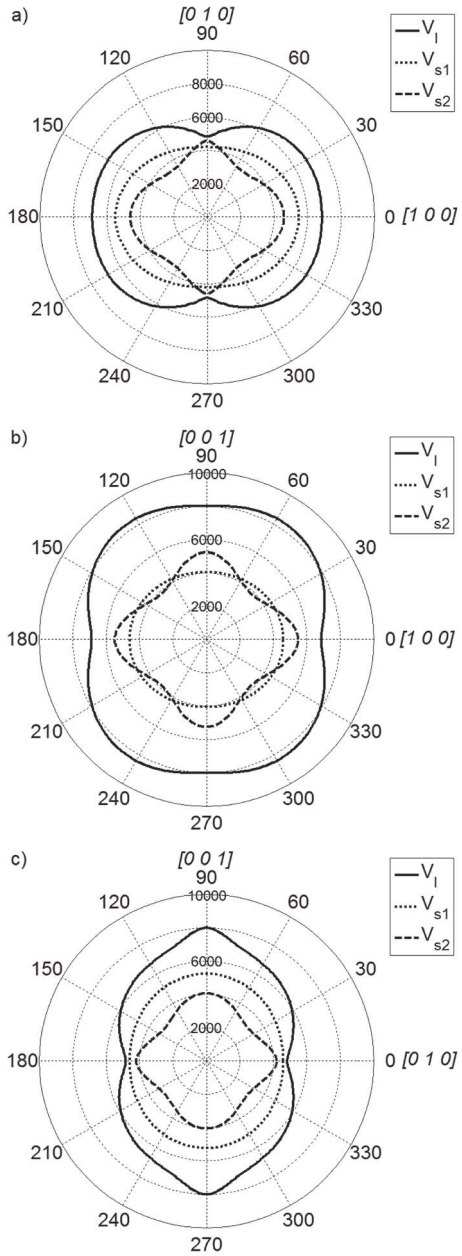

FIG. 5. Orientational dependence of the longitudinal velocity (m/s) v_l and the two shear velocities v_{s1} and v_{s2} in the (a) *XY*-plane, (b) *XZ*-plane, and (c) *YZ*-plane.

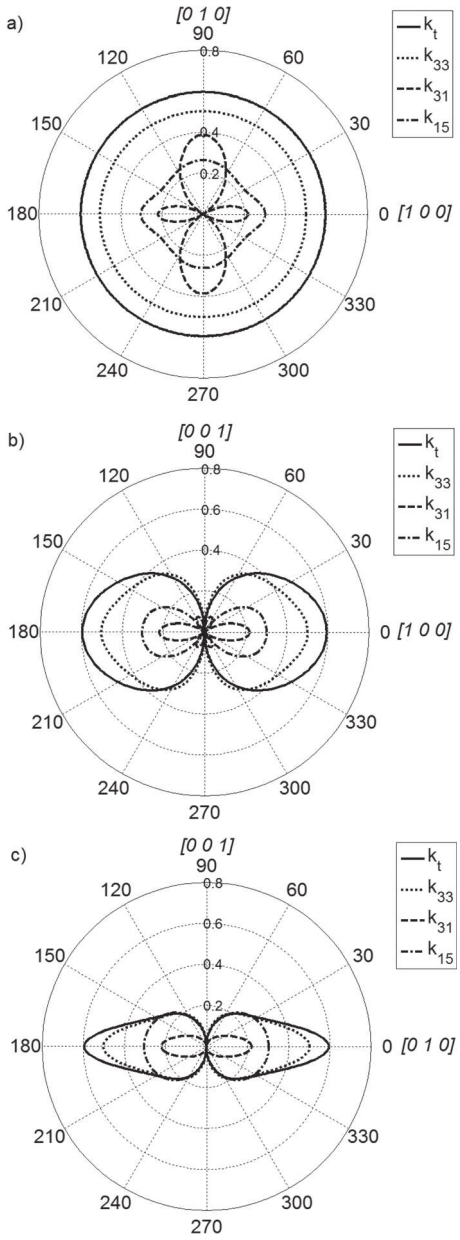

FIG. 6. Orientational dependence of the coupling coefficients (%) k_t, k_{33}, k_{31}, and k_{15} in the (a) *XY*-plane, (b) *XZ*-plane, and (c) *YZ*-plane.

values are constant for the *Z*-axis rotation. The two others are orientation dependent. In Figs. 6(b) and 6(c), k_t and k_{33} are equal to zero for a 90° rotation because the single crystal does not exhibit the spontaneous polarization in the *X*- and *Y*-directions.

IV. CONCLUSION

The $KNbO_3$ single crystal characterized here has a perovskite structure with orthorhombic mm2 symmetry at room temperature. From an original piece with dimensions of $10 \times 10 \times 3\,mm^3$ and a (YXt)–45° cut, several samples were cut to obtain the full set of dielectric, elastic, and piezoelectric constants. The consistency of the delivered database was a key point and to reach this objective a quantification criterion (to be minimized) of this consistency was first defined and an optimization was performed using a genetic algorithm. The main advantage of this algorithm is that it is practically insensitive to the choice of initial data; more precisely, it is only necessary to restrain the search space. The final value of this quantification criterion was compared with other values calculated from databases already published for similar composition.[12] According to this criterion, results show that a better consistency is obtained with our set of parameters.

Direct measurements confirmed good electromechanical performance for the thickness mode with a k_t of approximately 60%. Moreover, the good stability of these properties as a function of frequency observed by Davis *et al.*[15] coupled with the high longitudinal wave velocity value makes this material suitable for some high-frequency applications such as medical imaging. Finally, the consistent complete set of parameters of this piezoelectric lead-free material will be of primary importance for numerical studies and design of

devices as future legislation is expected to restrict the use of lead-based compositions in several countries.

ACKNOWLEDGMENTS

This work was supported by the French Research Agency (ANR HYPERCAMPUS Mat&Pro 2010) and the European Union (FEDER Funds).

[1]B. Jaffe, W. R. Cook, and H. Jaffe, *Piezoelectric Ceramics* (Academic Press, 1971).
[2]S. E. Park and T. R. Shrout, J. Appl. Phys. **82**, 1804 (1997).
[3]J. Rödel, W. Jo, K. T. P. Seifert, E.-M. Anton, T. Granzow, and D. Damjanovic, J. Am. Ceram. Soc. **92**, 1153 (2009).
[4]E. Ringgaard and T. Wurlitzer, J. Eur. Ceram. Soc. **25**, 2701 (2005).
[5]N. M. Hagh, B. Jadidian, E. Ashbahian, and A. Safari, IEEE Trans. Ultrason. Ferroelectr. Freq. Control **55**, 214 (2008).
[6]A. Safari, M. Abazari, K. Kerman, N. Marandian-Hagh, and E. K. Akdoğan, IEEE Trans. Ultrason. Ferroelectr. Freq. Control **56**, 1586 (2009).
[7]S. Wada, K. Yako, H. Kakemoto, T. Tsurumi, and T. Kiguchi, J. Appl. Phys. **98**, 014109 (2005).
[8]L. Katz and H. D. Megaw, Acta Crystallogr. **22**, 639 (1967).
[9]S. D. Phatak, R. C. Srivastava, and E. C. Subbarao, Acta Crystallogr., Sect. A **28**, 227 (1972).
[10]E. Wiesendanger, Ferroelectrics **6**, 263 (1973).
[11]T. Fukuda, H. Hirano, Y. Uematsu, and T. Ito, Jpn. J. Appl. Phys., Part 1 **13**, 1021 (1974).
[12]M. Zgonik, R. Schlesser, I. Biaggio, E. Voit, J. Tscherry, and P. Günter, J. Appl. Phys. **74**, 1287 (1993).
[13]K. Nakamura and Y. Kawamura, IEEE Trans. Ultrason. Ferroelectr. Freq. Control **47**, 750 (2000).
[14]K. Nakamura, T. Tokiwa, and Y. Kawamura, J. Appl. Phys. **91**, 9272 (2002).
[15]M. Davis, N. Klein, D. Damjanovic, N. Setter, A. Gross, V. Wesemann, S. Vernay, and D. Rytz, Appl. Phys. Lett. **90**, 062904 (2007).
[16]ANSI/IEEE Standard on Piezoelectricity, IEEE Trans. Ultrason. Ferroelectr. Freq. Control **43**, 717 (1996).
[17]FEE, see http://www.fee-io.de, 2014.
[18]H. Cao, V. H. Schmidt, R. Zhang, W. Cao, and H. Luo, J. Appl. Phys. **96**, 549 (2004).
[19]V. Yu. Topolov and C. R. Bowen, J. Appl. Phys. **109**, 094107 (2011).
[20]T. Ikeda, *Fundamentals of Piezoelectricity* (Oxford University Press, New York, 1996).
[21]J. H. Holland, *Adaptation in Natural and Artificial Systems* (University of Michigan Press, Ann Arbor, 1975).
[22]MATLAB 7.14.0 (R2012a), *Global Optimization Toolbox* (The MathWorks Inc., Natick, Massachusetts, United States, 2012).
[23]V. I. Aleshin and I. P. Raevski, J. Appl. Phys. **113**, 224105 (2013).
[24]R. G. Leisure and F. A. Willis, J. Phys.: Condens. Matter **9**, 6001 (1997).
[25]H. Ogi, Y. Kawasaki, M. Hirao, and H. Ledbetter, J. Appl. Phys. **92**, 2451 (2002).
[26]T. Delaunay, E. L. Clezio, M. Guennou, H. Dammak, M. P. Thi, and G. Feuillard, IEEE Trans. Ultrason. Ferroelectr. Freq. Control **55**, 476 (2008).
[27]S. Li, L. Zheng, W. Jiang, R. Sahul, V. Gopalan, and W. Cao, J. Appl. Phys. **114**, 104505 (2013).
[28]L. Zheng, X. Huo, R. Wang, J. Wang, W. Jiang, and W. Cao, CrystEngComm **15**, 7718 (2013).
[29]E. Sun and W. Cao, Prog. Mater. Sci. **65**, 124 (2014).
[30]C. Bantignies, E. Filoux, P. Mauchamp, R. Dufait, M. Pham Thi, R. Rouffaud, J. Gregoire, and F. Levassort, in *2013 IEEE International Ultrasonics Symposium (IUS)* (IEEE, 2013), pp. 785–788.
[31]R. E. Newnham, D. P. Skinner, and L. E. Cross, Mater. Res. Bull. **13**, 525 (1978).
[32]W. A. Smith and B. A. Auld, IEEE Trans. Ultrason. Ferroelectr. Freq. Control **38**, 40 (1991).
[33]D. Royer and E. Dieulesaint, *Elastic Waves in Solids I: Free and Guided Propagation* (Springer-Verlag Berlin, 1999).